Article

Bioactive Efficacy of Identified Phytochemicals Solasodine, Lupeol and Quercetin from *Solanum xanthocarpum* against the RgpB Protein of *Porphyromonas gingivalis*—A Molecular Docking and Simulation Analysis

Deepavalli Arumuganainar [1], Gopinath Subramanian [2,*], Santhosh Basavarajappa [3,*], Mohamed Ibrahim Hashem [3], Kurumathur Vasudevan Arun [4], Subbusamy Kanakasabapathy Balaji [5], Pradeep Kumar Yadalam [6], Baskar Venkidasamy [7] and Ramachandran Vinayagam [8,*]

[1] Department of Periodontics, Ragas Dental College and Hospital, Chennai 600119, Tamil Nadu, India; deeps.271@gmail.com
[2] Department of Pharmaceutics, Sri Ramachandra Faculty of Pharmacy, Chennai 600116, Tamil Nadu, India
[3] Dental Health Department, College of Applied Medical Sciences, King Saud University, Riyadh 11433, Saudi Arabia; mihashem@ksu.edu.sa
[4] Department of Periodontics, Amrita School of Dentistry, Ernakulam 682041, Kerala, India; arun_kurumathur@yahoo.co.in
[5] Department of Periodontics, Sri Ramachandra Dental College, Chennai 600116, Tamil Nadu, India; balajisk@sriramachandra.edu.in
[6] Department of Periodontics, Saveetha Dental College and Hospital, SIMATS, Chennai 600077, Tamil Nadu, India; yadalam1980@gmail.com
[7] Department of Oral and Maxillofacial Surgery, Saveetha Dental College and Hospital, SIMATS, Chennai 600077, Tamil Nadu, India; baskarbt07@gmail.com
[8] Department of Biotechnology, Institute of Biotechnology, Life and Applied Sciences, Yeungnam University, 280 Daehak-ro, Gyeongsan 38541, Gyeongbuk, Republic of Korea
* Correspondence: gopinath.s@sriramachandra.edu.in (G.S.); santhosh@ksu.edu.sa (S.B.); rambio85@gmail.com (R.V.)

Abstract: Periodontal diseases are highly prevalent oral conditions associated with severe complications in the oral cavity. These inflammatory diseases are caused by the oral microbiome and are influenced by several factors, such as aging, tobacco usage, systemic illness and inadequate oral hygiene. Plant-derived phytochemicals are extensively utilized in managing various periodontal diseases due to the presence of antioxidant, anti-inflammatory and antibacterial activities. Plant materials have shifted attention from conventional medicine to indigenous medicine. *Solanum xanthocarpum* is a medicinal herb found in India. It exhibits various pharmacological properties essential for periodontal disease prevention and management. The current work analyzes various pharmacological properties of *S. xanthocarpum* aqueous extract. The *S. xanthocarpum* extracts' antioxidant, anti-inflammatory and anti-microbial properties were ascertained by DPPH assay, HRBC membrane stabilization assay and disk diffusion assay, respectively. *S. xanthocarpum*'s active phytochemical components were detected using gas chromatography–mass spectrometry (GC-MS) estimation. Furthermore, molecular docking and simulation analysis were conducted to determine the interaction between phytocompounds and the RgpB protein of *Porphyromonas gingivalis*. Phytocompounds possessing anti-microbial, antioxidant and anti-inflammatory properties were detected through GC-MS estimation. The molecular docking and simulation analysis revealed the inhibitory mechanisms of the phytocompounds Solasodine, Lupeol and Quercetin against arginine-specific gingipain RgpB protein. Insilico analysis revealed that Lupeol had the highest binding energy of −263.879 Kcal/mol among the phytocompounds studied, followed by Solasodine with a binding energy of −102.457 Kcal/mol and Quercetin with a binding energy of 33.6821 Kcal/mol. The study revealed that *S. xanthocarpum* has significant potential as an herbal remedy for preventing and treating periodontal diseases. This may facilitate drug development in the future.

Keywords: periodontal disease; Porphyromonas gingivalis; RgpB protein; *Solanum xanthocarpum*; molecular docking

1. Introduction

Periodontal diseases encompass widespread inflammatory conditions that affect the tooth-supporting structures. Clinically, they are associated with loss of gingival connective tissue attachment, destruction of the periodontal ligament and alveolar bone loss [1]. Microbial communities mediate periodontal disease onset and progression. These communities, upon interaction with the host defense system, produce dense immune-inflammatory infiltration and may eventually lead to tooth loss if not appropriately intervened. Biofilm accumulation and oral microbiota are the major contributors; however, modifiable risk factors such as diabetes mellitus, smoking, obesity, osteoporosis, calcium and vitamin D deficiencies, and other non-modifiable factors such as genetic polymorphism can also be leading contributors [2].

The disease persists in active and quiescent stages. If left unaddressed, it results in tooth loss but also affects esthetics, masticatory efficacy and quality of life [3]. Thus, removing plaque biofilm by the judicious use of toothbrushes and dental floss has been the mainstay of controlling the disease. However, inadequate oral hygiene measures are considered a significant risk factor for periodontal disease. It is reported that fair to poor oral hygiene practices may account for a two- to fivefold increase in periodontitis [4]. Mechanical debridement is the standard therapy for periodontal diseases to ward off the pathogenic microbial biofilm [5]. In addition, chemical plaque control agents and/or antimicrobial agents play adjunctive roles in eliminating pathogenic microflora. However, chlorhexidine mouth rinse (the gold standard) causes hypersensitivity, staining of the tooth surface, mucosal irritation and altered taste [6]. Exponentially rising antibiotic resistance has also warranted the development of novel antibacterial agents without adverse effects [7].

Phyto-therapy for oral health has received a lot of attention lately. Various clinical trials involving herbal concoctions have been conducted due to the development of anti-microbial resistance, hypersensitivity and gastric intolerance to conventional antimicrobials [8,9]. Plants exhibit anti-inflammatory, anti-microbial and antioxidant properties. The utilization of these herb properties can result in the secure and efficient management of periodontal disease [10,11]. *Solanum xanthocarpum (Sx)* is generally recognized as the yellow berried nightshade and is a perennial herb, prickly with a woody base. The plant is found all over India, mainly in dry places and wastelands. The plant possesses various medicinal properties, including antipyretic, antioxidant, anti-microbial, anti-tumor, anti-inflammatory, hepatoprotective, anti-allergic, immunomodulatory and anti-filarial activity [12–14]. The anti-microbial properties of *Sx* on cariogenic oral microbial flora, namely, streptococcus mutans, actinomyces viscosus and lactobacillus, have been evaluated and have shown statistically significant antibacterial activity when compared to the positive control, chlorhexdine [13].

The current study aims to assess the antibacterial efficacy of *Sx* fruit extract against periodontal pathogens isolated from dental plaque biofilm. It also aimed to estimate the antioxidant and anti-inflammatory properties. In addition, the investigation focuses on identifying bioactive phytochemicals from *Sx* extracts by GC-MS estimation. Moreover, insilico molecular docking and simulation analysis of the most potent bioactive compounds, Solasodine, Lupeol and Quercetin, were identified from our analysis. These compounds were targeted against the RgpB protein of *Porphyromonas gingivalis*, which is considered the keystone pathogen involved in periodontal disease pathogenesis [15].

2. Materials and Methods

2.1. Collection of S. xanthocarpum Fruits and Extraction

S. xanthocarpum fruiting bodies were harvested from different parts of Chennai and Tirunelveli, Tamil Nadu, India. A taxonomist botanically identified the herbal plant samples, authenticated it, and a voucher specimen was submitted to the Plant Anatomy Research Center in Chennai, Tamil Nadu, India, for future reference (no. PARC/2021/4483). The study was also approved by the Institutional Ethics Committee of Sri Ramachandra Institute of Higher Education and Research (Deemed to be University), Chennai, Tamil Nadu, India

(IEC/21/JUN/163/45), and Ragas Dental College and Hospital (No: 20170762). The collected plant materials were cleaned in running tap water, shade-dried, powdered and stored for further analysis. Soxhlet extraction was carried out for 7 h and 20 cycles using hexane, ethyl acetate, ethanol, chloroform and distilled water separately to obtain a 20% yield. At 40 °C, the final preparations were filtered and concentrated using a rotary evaporator until they were completely desiccated. The final dried extracts were sterilized overnight by UV irradiation and verified for sterility on the nutrient agar plates. The extracts were preserved at 4 °C until further usage.

2.2. Preliminary Screening of Activities of Solanum xanthocarpum Extracts

2.2.1. Antioxidant Assay of Crude Extract

The free radical scavenging property of different solvent extracts was tested against 1,1-diphenyl-2-picrylhydrazyl (DPPH) [16]. The sample stock solution was diluted in methanol to final concentrations of 20, 40, 60, 80 and 100 µg/mL. One mL sample of these concentrations was mixed with the same quantity of 0.1 mM methanolic solution of DPPH (0.39 mg in 10 mL methanol). Equal quantities of DPPH and methanol were added and used as the control. Gallic acid of concentrations viz., 2, 4, 6, 8, 10, 12, and 14 µg/mL in distilled water was used as the standard. After 20 min of incubation in the dark, the absorbance was measured at 517 nm. The experiment was performed in triplicates. The following equation was used to compute the percentage of scavenging: % DPPH radicalscavenging (% of inhibition) = [(Absorbance of control − Absorbance of test Sample)/(Absorbance of control)] × 100.

2.2.2. Anti-Inflammatory Assay of Crude Extract

The anti-inflammatory activity of the plant extracts was estimated using the human red blood cell membrane stabilization (HRBC) assay [17]. Blood from human volunteers was collected, combined with Alsever solution in equal amounts, and centrifuged with isosaline. The supernatant was collected after the samples were centrifuged at 2500 rpm for 5 min. The cell suspension was centrifuged at 2500 rpm for 5 min after being cleaned with sterile saline solution (0.9 percent w/v NaCl). This was carried out three times to obtain the clear, colorless supernatant. The cellular component was employed in the assay after being reconstituted to a 40% suspension (v/v) in phosphate-buffered saline (10 mM, pH 7.4). The plant extracts were prepared in 250, 500 and 1000 mg/mL in different solvents (ethyl acetate, hexane, distilled water, ethanol and chloroform). To 1 mL of HRBC suspension, an equal quantity of plant extract prepared in respective solvents was added. It was incubated at 37 °C for 30 min and centrifuged at 3000 rpm for 20 min. The hemoglobin content was measured spectrophotometrically at 560 nm from the supernatant solution. The following equation was used to compute the percentage of hemolysis:

$$\text{Hemolysis}(\%) = \frac{\text{OD of Test}}{\text{OD of Control}} \times 100$$

The percentage of membrane protection can be hence calculated using the equation:

$$\text{Protection}(\%) = 100 - \frac{\text{OD of Test}}{\text{OD of Control}} \times 100$$

where, OD of test is the optical density of the test sample in hypotonic solution and OD of control is the optical density of the Alsever solution with blood and without the plant extracts (negative control).

2.2.3. Antibacterial Activity of the Crude Extract

The microbial plaque samples were collected from patients diagnosed with stage III or IV, grade A periodontitis according to the Periodontal and Peri-Implant Diseases classification of the 2017 World Workshop at Ragas Dental College and Hospital, Chennai, Tamil Nadu, India [18]. The patients' written informed consent for sample collection was

obtained. Subgingival plaque samples were collected using sterile curettes in Eppendorf tubes, which contained phosphate-buffered saline solution and were stored at $-20\ ^\circ$C until processing.

The antibacterial activities of the crude plant extracts were screened against the plaque microflora using the disc diffusion method. A colony of bacteria was selected using a sterile loop, and it was suspended in 10 mL of nutrient broth to prepare a standardized bacterial suspension. In sterile plates, nutrient agar medium was deposited aseptically, and a bacterial inoculum was developed. The known concentrations of the test sample solutions were prepared by dissolving the measured number of samples in the solvent. Dried filter paper discs were prepared and loaded with different solvent extracts of the test substance using a micropipette. Discs with the test material were placed in the nutrient agar medium uniformly containing the bacterial inoculum. The culture plates were then kept at 37 $^\circ$C for 20 min for diffusion. The culture plates were then incubated at 37 $^\circ$C for 24 h. The antibacterial activity of the test substances was assessed by measuring the inhibition zones (measured in millimeters) formed around the discs.

2.3. Column Chromatographic Fractionation of the Aqueous Extract

2.3.1. Separation and Identification of Bioactive Compounds

Silica gel (100–200 mesh size) was kept in a hot air oven at 110 $^\circ$C for 60 min to activate the silica. The slurry was made with hexane and stirred vigorously to remove the air. Cotton was used to tightly pack the glass column (40 mm × 600 mm) and prevent silica gel from draining during elution. The silica gel slurry was poured into the column using a glass funnel and the knob was opened with moderate tapping for uniform packing. The knob was closed and the setup was allowed to stand for a few hours with a small amount of solvent to remain over the silica gel packing to prevent the column from forming air cracks. A circle of filter paper was placed at the top of the column to avoid surface disturbance during consequent loading. The aqueous extract was poured into the column through a glass funnel and allowed to settle. The elution was initiated with a mobile phase of a nonpolar solvent, hexane, and the fractions were collected in test tubes. The flow rate of elution was 1 mL/min with a gradient of 1000 mL of hexane/ethyl acetate (9:1 to 0:10). At last, the column was eluted with methanol. Each fraction was subjected to activity-based screening. The fractions that demonstrated the maximum potency for antibacterial, antioxidant and anti-inflammatory activities were chosen for phytochemical characterization along with the aqueous crude extract.

2.3.2. GC-MS Analysis of *S. xanthocarpum*

The characterization was undertaken using Agilent Technologies and GC-MS equipped with an Elite-1 fused silica capillary column (30 mm × 250 μm ×0.25 μm) containing HP-5MS 5% phenyl methyl silox, 60 $^\circ$C. An electron impact ionization system with 70 EV of ionizing energy was used for the GC-MS detection. Helium gas (99.999%) was used as the carrier at a constant flow rate of 1 mL/min and an injection volume of 1 μL was used with an injector temperature of 250 $^\circ$C and ionsource temperature of 280 $^\circ$C. The oven temperature changed from 220 $^\circ$C to 200 $^\circ$C at a rate of 10 $^\circ$C/min, followed by an increase from 200 $^\circ$C to 280 $^\circ$C at a rate of 5 $^\circ$C/min. The temperature was then held at 280 $^\circ$C for 9 min. Mass spectra fragments were scanned from 40 to 700 Amu at intervals of 0.5 s. The total GC running time was 120 min. The average peak area was compared to that of the total area to estimate the relative percentage of each component. A Mass Hunter program was adopted to manage mass spectra and chromatograms. Mass spectrum GC-MS was interpreted using the National Institute of Standard and Technology (NIST) database with more than 100,000 patterns.

2.4. Molecular Docking Analysis

To understand the inhibitory mechanisms of phytocompounds, namely, Solasodine, Lupeol and Quercetin from the *Sx* extract, molecular docking analysis was carried out

against the RgpB protein of *Porphyromonas gingivalis*. *P. gingivalis* is an opportunistic pathogen established in up to 85% of periodontitis cases [19]. It has been reported that *P.gingivalis* impairs innate immunity and alters the growth and maturity of the whole biofilm, eliciting a destructive pattern in the host–microbial homeostatic interaction in the periodontium. Hence, it has been considered a keystone pathogen among the disease-aggravating periodontopathic microflora leading to oral microbiome dysbiosis and periodontitis development [15]. This pathogen possesses several virulence factors [19] such as the lipopolysaccharide, capsule, fimbriae, proteolytic enzymes, surface ligands and, most importantly, cysteine proteinases, viz., gingipains, which include arginine-specific gingipains (Rgp, including RgpA and RgpB) and lysine-specific gingipain (Kgp) [20]. Although the gingipains are involved in several mechanisms of destruction of the periodontal structures, the RgpB protein is known to exhibit some distinct mechanisms of destruction. A study reported that RgpB inactivated elafin, which is a strong proteinase-3 inhibitor and neutrophil elastase secreted by the epithelial cells at the inflamed sites. This inactivation embodies the organisms' specific adaptation to disrupt the balance between the protease and its inhibitors at the infected sites and eventually promotes the degradation of the proteins and the generation of a rich supply of nutrients for the organism to thrive [21]. Moreover, another study demonstrated that RgpB protein can be considered as a specific biomarker for the detection of this pathogen. Hence, the RgpB protein was used as a target of the phytocompounds in this study [22].

The complete structure of Gingipain R2 (RgpB) (Uniprot ID: P95493) of *P. gingivalis* was predicted by AlphaFold using the sequence retrieved from Uniprot [23,24]. Using the CHARMm forcefield, the protein was subjected to energy minimization until a satisfactory gradient tolerance was reached. The stereochemical features of the modelled protein were verified using the PROCHECK server [25]. The structures of ligand molecules with proven pharmacological activity, such as antioxidant, anti-inflammatory and antimicrobial properties identified from GC-MS analysis, were retrieved from the PubChem database [26]. The molecules were prepared using ligands tools and the structures were minimized in energy using CHARMm forcefield. The protein and ligand molecules were prepared in BIOVIA Discovery Studio v.2022.

The binding of RgpB protein with the ligand molecules was further investigated using a molecular docking approach. Blind docking was carried out using CHARMm-based molecular docking module of BIOVIA Discovery Studio v.2022 to generate docking poses of the ligands. Hundreds of ligand conformations were produced from the initial ligand structure for all three ligands under high-temperature (1000 K) MD simulation (1000 steps) followed by random rotations. The ligand poses were generated by dynamics-based simulated annealing refinement. Around 30 different binding poses were sorted and ranked based on CDOCKER energy. The final docked conformations and interactions were visualized using the 2D representation feature of BIOVIA Discovery Studio v.2022.

2.5. Molecular Dynamics Simulation of Apo-Protein and Protein–Ligand Complexes

The apo Gingipain R2 protein and ligand-docked protein complexes' poses were chosen based on their binding energies from the previous docking analysis. The structures were subjected to molecular dynamics and simulation (MDS) independently. MDS runs were carried out in Gromacs 2019.4 version using a Gromos54a7 forcefield [27]. The topology files for the ligand structures were produced using the PRODRG2 server [28]. All 4 systems were solvated in cubic boxes with counter-ions and water molecules. The systems utilized the steepest minimization algorithm for energy minimization. The first equilibration was conducted using NVT ensembles with a 1 ns V-scale thermostat. The second equilibration step was carried out using an NPT ensemble with a Parrinello–Rahman barostat for 1 ns. During the simulation runs, the protein backbone was restrained and counter-ions and solvent molecules were allowed to move. A final production MD of 50 ns under periodic boundary conditions was carried out for all four systems independently. The results were analyzed according to root mean square deviation (RMSD), the radius of

gyration (Rg), root mean square fluctuation (RMSF), principal component analysis (PCA) and hydrogen bonds. Comprehensive intermolecular interactions were analyzed only for the complex systems using the MM/PBSA approach [29]. For each complex, 1000 snapshots were extracted from the trajectories and used for the calculation of binding energy using the following formula:

$$\Delta Gbind = <GProtein\text{-}Ligand\ complex - GProtein - GLigand>$$

where, GProtein-Ligand complex, GProtein and GLigand are the free energies of the complex, protein and ligand, respectively.

3. Results and Discussion

3.1. Antioxidant Activity of S. xanthocarpum Extracts

The fruit body *Sx* extracts at various concentrations were tested using the DPPH assay. Figure 1a displays the IC50, which represents the minimum extract concentration needed to reduce the target substrate by 50%. Solvent extracts exhibited potent antioxidant properties. Among them, at the concentration of 100 µg/mL, the aqueous extract showed the maximum antioxidant activity of 82.32% with an IC_{50} of 55.74 µg/mL, while the hexane extract demonstrated the least activity of 71.29% with an IC_{50} of 69.24 µg/mL (Figure 1b). The results indicate that the *Sx* extracts demonstrated free radical scavenging effects on DPPH radicals. These findings corroborate the results of Sridevi Muruhan et al., who found that Solanum surettense leaf extract, at comparable concentrations, demonstrated strong antioxidant properties [30]. Their DPPH assay demonstrated the IC_{50} value of *S. surettense* ethanolic leaf extract to be 55.62 µg/mL. This was equivalent to that of our present study's aqueous extract. Another study also suggested that different extracts of *Sx* fruits demonstrated about 80% of free radical scavenging potential at 250 µg/mL [12]. In another report, the methanolic extract of the aerial parts of S. surettense displayed the highest activity of 83.15% at 150 µg/mL, which supported and validated the current findings in which the aqueous extract exhibited a similar value of 82.32% at 100 µg/mL [31]. The potent antioxidant activity of the *Sx* fruit extracts could be attributed to flavonoids and phenolic components in the extract. Flavonoids also possess free radical scavenging properties in their broad biological spectrum [32]. In the present study, quercetin, one of the major flavonoids, was isolated and identified using GC-MS analysis.

3.2. Anti-Inflammatory Activity of S. xanthocarpum Extracts

Synthetic diclofenac sodium exhibited 72.14% anti-inflammatory activity at a concentration of 50 µg/mL, as determined by the assay results. The anti-inflammatory activity of five extracts (Figure 1c) was evaluated at a concentration of 1000 µg/mL. The ethanol extract exhibited the highest activity (71.88%), followed by the aqueous extract (61.16%), hexane extract (57.68%), ethyl acetate extract (57.39%) and chloroform extract (53.33%). The results indicate that *Sx* fruit extracts can be utilized as anti-inflammatory agents. Such potential could be attributed to stigmasterol and triterpenes such as lupeol present in *Sx*. Previous studies have also shown that stigmasterol and lupeol are potent anti-inflammatory agents [33,34]. Lupeol targets key molecular pathways involving nuclear factor κ B (NFκB), Wnt/β-catenin, etc. [34]. Our current findings validate the use of *Sx* by traditional practitioners for managing inflammation-related diseases. Efficient and valuable anti-inflammatory agents are necessary for successful drug development and to validate the use of medicinal plants by traditional practitioners.
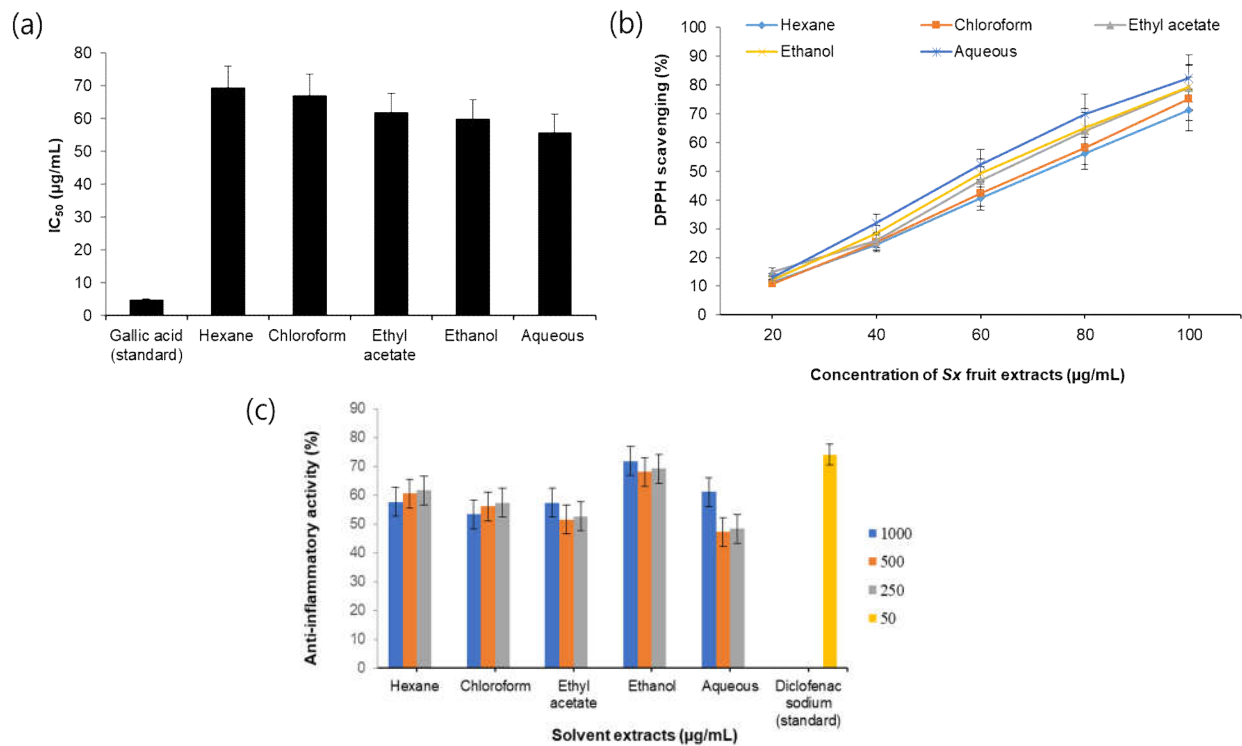
Figure 1. (**a**) IC$_{50}$ value (μg/mL) of different solvent extracts of *S. xanthocarpum*. (**b**) DPPH free radical scavenging activity of different solvent extracts of *S. xanthocarpum*. (**c**) Anti-inflammatory activity of different solvent extracts of *S. xanthocarpum*.

3.3. Antibacterial Activity of S. xanthocarpum Extracts

The susceptibility of plaque microbiota to various solvent extracts was determined by the presence of a zone of inhibition around the discs. Almost all *Sx* extracts except hexane extract showed significant antibacterial activity against plaque microbiota. The aqueous and chloroform extracts exhibited the highest zone of inhibition against microbes in most samples, with a maximum of 15 mm. This was compared to the standard antibiotic, Streptomycin 10 μg/vol. (See Figures 2 and 3). Several previous studies have also reported the significant anti-microbial activity of *Sx* extracts against an array of pathogens [35].

The anti-microbial activity could be attributed to alkaloids, glycosides, tannins, terpenoids, etc. These substances could have penetrated the bacterial cell wall and either suppressed or lysed the organism. A study by Abbas et al. evaluated the anti-microbial activity of various solvent extracts of *Sx* fruits at 20 mg/mL and demonstrated that the aqueous extract and methanol extract showed the maximum anti-microbial efficacy against Gram-negative organisms, *E. coli* and *S. typhi*, and Gram-positive organisms, *S. aureus* and *Micrococcus luteus*, in comparison to the other extracts [36]. The maximum efficacy of the aqueous extract indicates that water was found to be most potent for extracting the highest percent of highly polar components present in *Sx* fruits. These results suggest that the extract made with solvents of higher polarity possess greater potential for antibacterial activity than those made with less polar solvents. The overall results of the antibacterial assay indicate that the microbes in the dental plaque samples were sensitive to all *Sx* extracts except hexane.
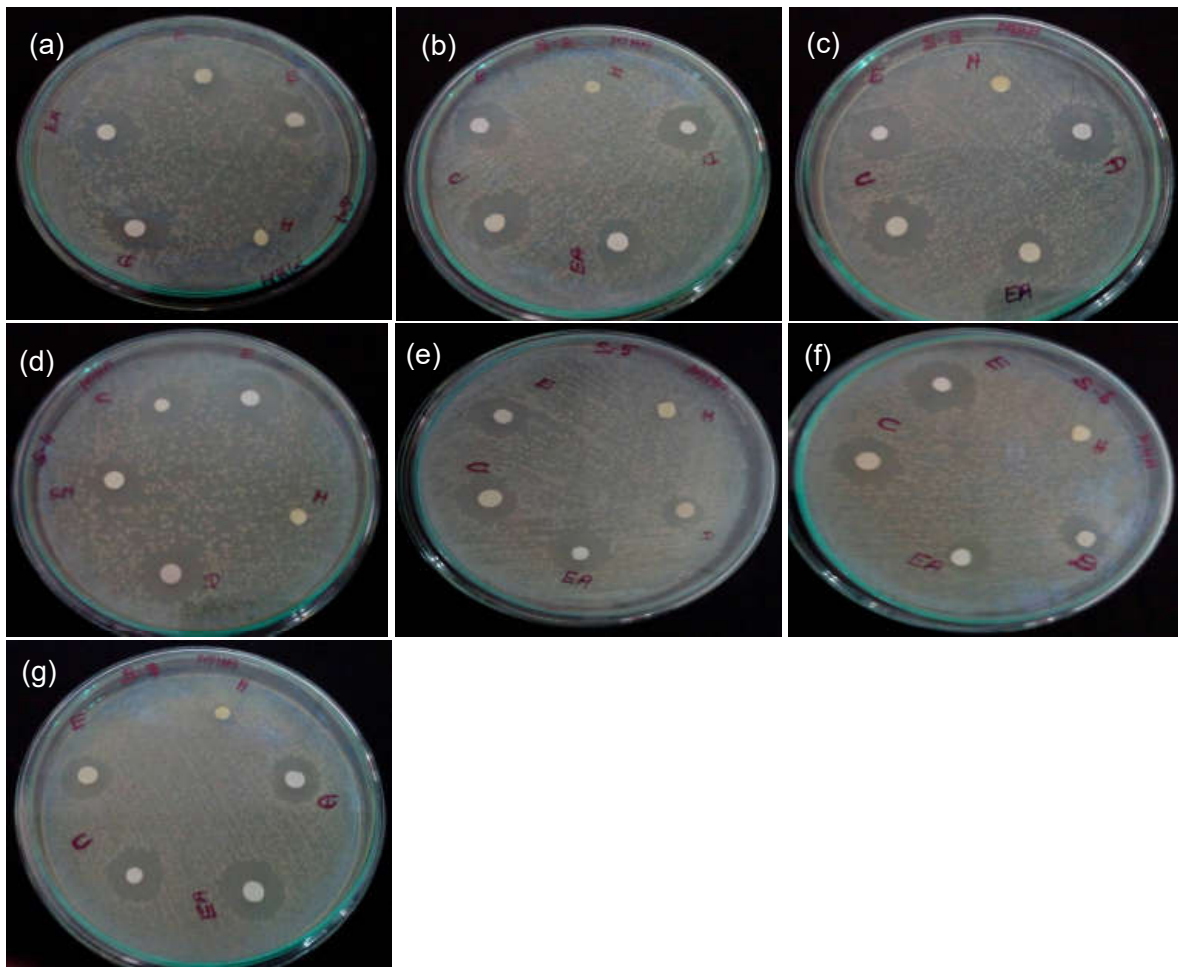
Figure 2. Antibacterial activity of different solvent extracts of *S. xanthocarpum* (**a–g**) Zone of inhibition observed in samples S1 to S7.H—hexane, D—distilled water/aqueous, EA—ethyl acetate, C—chloroform, E—ethanol.
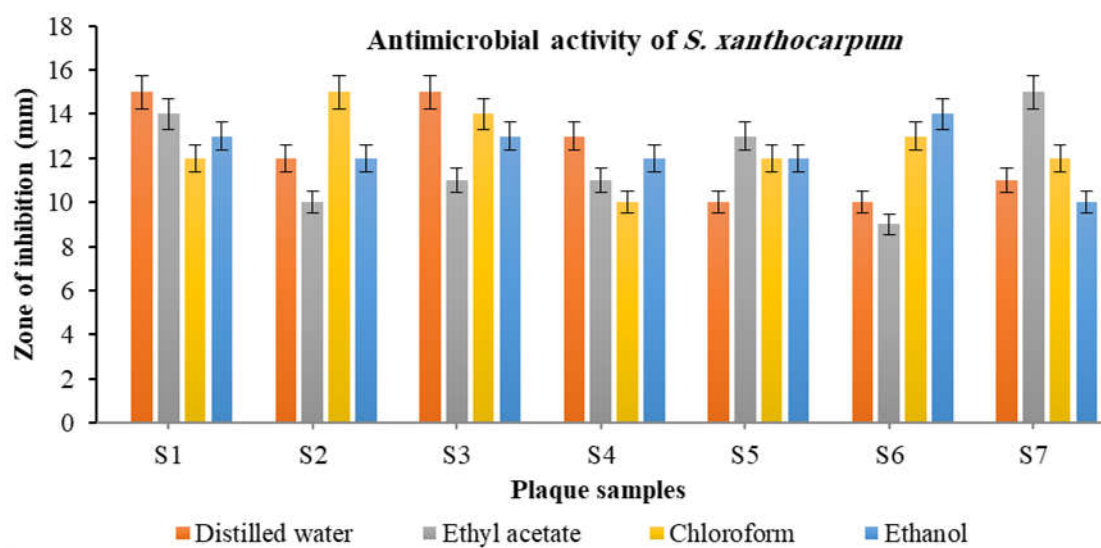

Figure 3. Antibacterial activity of different solvent extracts of *S. xanthocarpum* shows the measurement in inhibition zones against bacteria from plaque biofilm.

3.4. Gas Chromatography–Mass Spectrometry (GC-MS) Analysis

The GC-MS chromatogram of the crude aqueous extract and subfractions of *Sx* (fractions 1 and 2) showed 15, 5 and 7 peak areas. These peaks were identified as bioactive phytochemicals based on their retention times, peak areas and height, as well as mass spectral fragmentation patterns that matched those of the NIST library compounds. See Figure 4 and Tables 1–3 for details. The crude extract showed the presence of various sterols such as Stigmasterol, Lanosterol and Taraxasterol. Stigmasterol is known for its anti-inflammatory activity [37]. Lanosterol accumulation increases the membrane's fluidity and the production of reactive oxygen species (ROS), thus activating phagocytosis and eliminating pathogens such as bacteria [38]. Taraxasterol is reported to possess anti-allergic, anti-inflammatory and antioxidant properties [39]. Phytol identified in the crude extract exhibits antioxidant activity [40]. The crude extract, which includes Quercetin, promotes balanced periodontal homeostasis by inhibiting inflammation. In addition, it promotes periodontal host and microbiome tissue homeostasis [41]. It also exhibits various beneficial effects on oral health as a preventive and therapeutic agent for dental caries [42]. The crude extract and selected fraction 1 contained Solasodine, which exhibits potent antioxidant, anti-inflammatory and anti-microbial properties [43]. A major component in fraction 2 was Lupeol, an active terpenoid involved in anti-inflammatory activities [34]. Based on the anti-microbial, anti-inflammatory and anti-oxidant potential, three compounds Solasodine (PubChem CID-5250), Quercetin (PubChem CID-5280343) and Lupeol (PubChem CID-259846) were chosen for further molecular docking analysis to target the RgpB protein of *P. gingivalis*.

Table 1. Phytochemical components identified in the aqueous crude extract of *S. xanthocarpum* by GC-MS analysis.

| S. No.	RT	Name of the Compound	Molecular Formula	MW	Peak Area %
1	5.329	Pyridine	C_5H_5N	79.0999	3.70
2	6.032	3-Hexen-2-one	$C_7H_{12}O$	112.1696	0.67
3	6.7544	2-Pentanone,4-Hydroxy-4-methyl-	$C_6H_{12}O_2$	116.1583	62.11
4	17.709	Diethyl phthalate	$C_{12}H_{14}O_4$	222.2372	1.54
5	20.457	Bicyclo[3.1.1]heptane,2,6,6-trimethyl-	$C_{10}H_{18}$	138.2499	2.07
6	21.307	Hexadecanoic acid, methyl ester	$C_{17}H_{34}O_2$	270.4507	3.22
7	23.021	9,12-Octadecadienoic acid (Z,Z)-, methyl ester	$C_{19}H_{34}O_2$	294.4721	2.97
8	23.080	9,12,15-Octadecatrienoic acid, methyl ester	$C_{19}H_{32}O_2$	294.4562	3.67
9	23.183	Phytol	$C_{20}H_{40}O$	296.5310	1.90
10	23.306	Octadecanoicacid, methylester	$C_{19}H_{34}O_2$	294.4721	1.00
11	23.705	Quercetin	$C_{15}H_{10}O_7$	302.2360	2.76
12	33.203	Stigmasterol	$C_{29}H_{48}O$	412.6908	1.72
13	34.003	Solasodine	$C_{27}H_{43}NO_2$	413.6331	8.63
14	35.221	Lanosterol	$C_{30}H_{50}O$	426.7174	2.08
15	35.437	Taraxasterol	$C_{30}H_{50}O$	426.7174	3.10
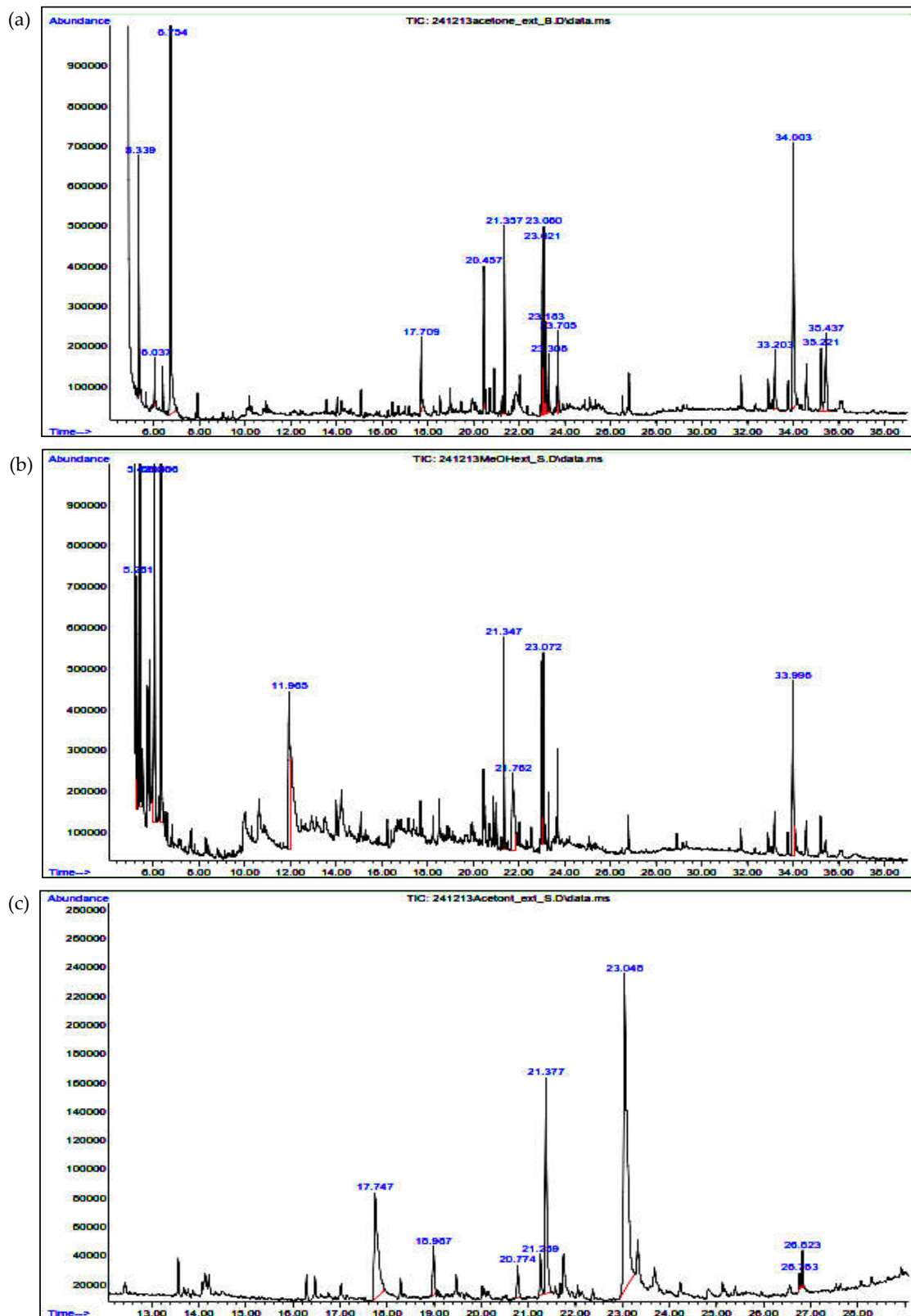
Figure 4. (**a**) GC-MS chromatogram formed by the aqueous crude extract of *S. xanthocarpum*. (**b**) GC-MS chromatogram formed by sub-fraction 1 of aqueous crude extract of *S. xanthocarpum*. (**c**). GC-MS chromatogram formed by the sub-fraction 2 of aqueous crude extract of *S. xanthocarpum*.

Table 2. Phytochemical components identified in the sub-fraction 1 of aqueous crude extract of *S. xanthocarpum* by GC-MS analysis.

S. No.	RT	Nameofthe Compound	Molecular Formula	MW	Peak Area %
1	11.965	1-Dodecene	$C_{12}H_{24}$	168.31	4.45
2	21.347	Hexadecanoic acid, methyl ester	$C_{17}H_{34}O_2$	270.4507	5.75
3	21.762	n-Hexadecanoicacid	$C_{16}H_{32}O_2$	256.4241	2.78
4	23.072	9,12,15-Octadecatrienoic acid, methyl ester	$C_{19}H_{32}O_2$	294.4562	4.87
5	33.996	Solasodine	$C_{27}H_{43}NO_2$	413.6331	4.41

Table 3. GC-MS analysis revealed the presence of phytochemical components in sub-fraction 2 of aqueous crude extract of *S. xanthocarpum*.

S. No.	RT	Nameofthe Compound	Molecular Formula	MW	Peak Area %
1	17.747	Diethyl phthalate	$C_{12}H_{14}O_4$	222.2372	9.36
2	18.967	Heptadecane	$C_{17}H_{36}$	240.4677	5.02
3	20.774	1-Nonadecene	$C_{19}H_{38}$	266.5050	3.68
4	21.209	Hexadecanoic acid, methyl ester	$C_{17}H_{34}O_2$	270.4507	4.25
5	21.337	n–Hexadecanoicacid	$C_{16}H_{32}O_2$	256.4241	18.49
6	23.045	9,12-Octadecadienoic acid (Z,Z)-, methyl ester	$C_{19}H_{34}O_2$	294.4721	26.16
7	26.623	Lupeol	$C_{30}H_{50}O$	426.7174	6.13

3.5. InSilico Analysis

3.5.1. Molecular Docking Using CDOCKER

Initially, the stereochemical quality of the modeled and energy-minimized protein structure of RgpB (Figure 5a) was checked by analyzing the overall and residue by residue geometry using the PROCHECK server. The residue distribution in the disallowed regions on the Ramachandran plot was around 0.3% (Table 4). Hence, the predicted structure was highly efficient for the docking study. The study analyzed the CDOCKER energy and binding site residues (Table 5) to determine the optimal binding mode of the ligands in the RgpB protein's active site. Based on the CDOCKER energy ranking, Quercetin was ranked first, followed by Lupeol and Solasodine. Lupeol favored Pi-Alkyl interactions within the binding site with Leu265, Tyr301, Ile535, Arg537, Leu574 and Ile608. Solasodine formed a single hydrogen bond with Arg263 and Pi-Alkyl interactions with Arg537, Leu574, Ile608 and Ile622. In addition, Lupeol also showed an intermolecular steric clash with Arg263. Quercetin favored hydrogen bonds with Glu235, Lys236, Glu237 and Arg537 and Pi-Alkyl interactions with Ile608 and Ile622. A closer look at the interacting residues revealed that Lupeol and Solasodine shared similar residues involved in Pi-Alkyl interactions. Arg537 was involved in the formation of Pi-Alkyl interactions with Lupeol and Solasodine, while it favored hydrogen bonds with Quercetin. Most residues showing interactions were conserved in all three ligand molecules, revealing that the binding site was favored by all three ligands (Figure 5b). The interaction patterns also revealed that non-bonded interactions were preferred by the ligands rather than conventional hydrogen bonds (Figure 6). The results of docking analysis revealed that all three compounds show binding preference towards RgpB protein. The further stability of the docked complexes was assessed using molecular simulation by comparing the ligand-bound protein complexes and free RgpB protein.
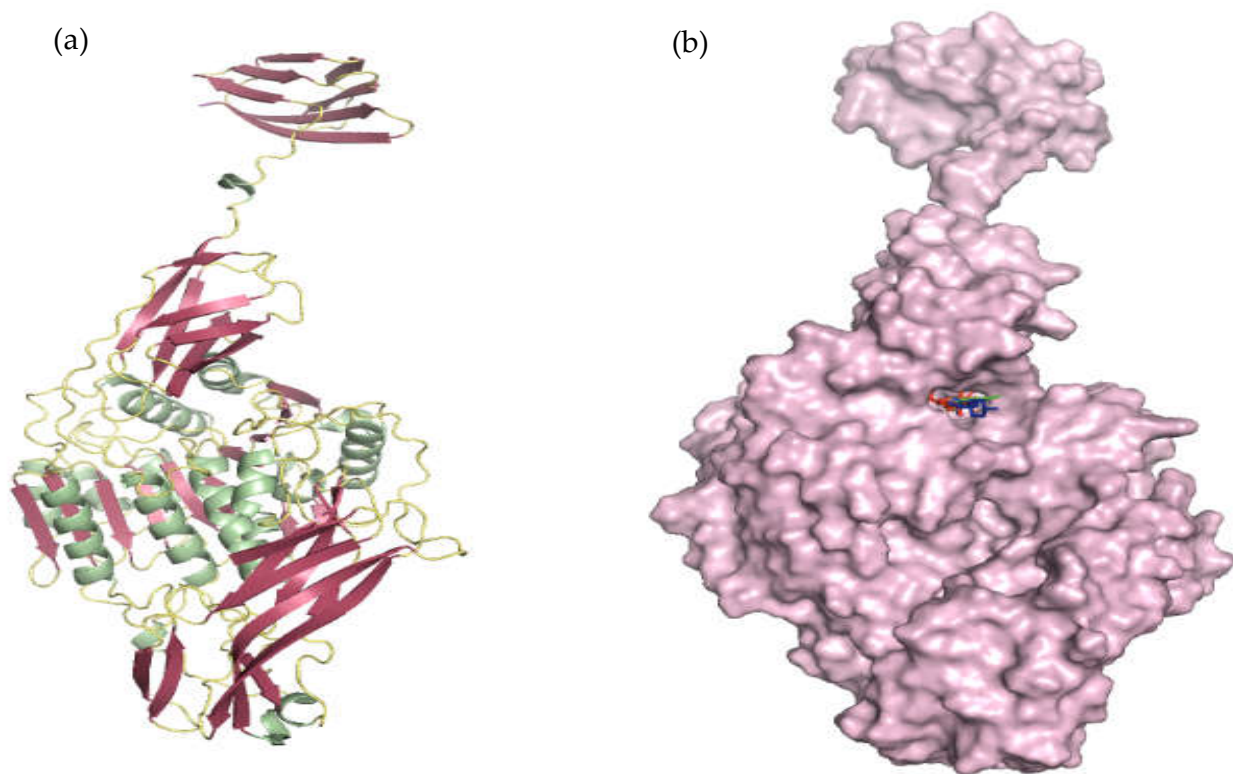
(a)

(b)

Figure 5. (**a**) Modeled and energy-minimized structure of RgpB protein shown in cartoon representation. (**b**) Structure of RgpB protein bound with the ligand molecules. The protein is shown as surface, and ligand molecules as sticks (Lupeol—red, Quercetin—green, Solasodine—blue).

Table 4. Ramachandran plot statistics of the modeled protein.

Region	Percentage of Residues (%)
Residues in the most favored region	89.2
Residues in additionally allowed region	9.8
Residues in the generously allowed region	0.6
Residues in the disallowed region	0.3

Table 5. CDOCKER energy of the ligand compounds.

Compounds	CDOCKER Energy (kcal/mol)
Lupeol	−263.879
Solasodine	−102.457
Quercetin	33.6821

3.5.2. Molecular Dynamics and Simulation Analysis

The molecular dynamic simulation further verified the stability of docked complexes and binding interactions. The apo-protein and ligand-anchored protein complexes were compared to understand the binding influence of all three ligands upon the protein.
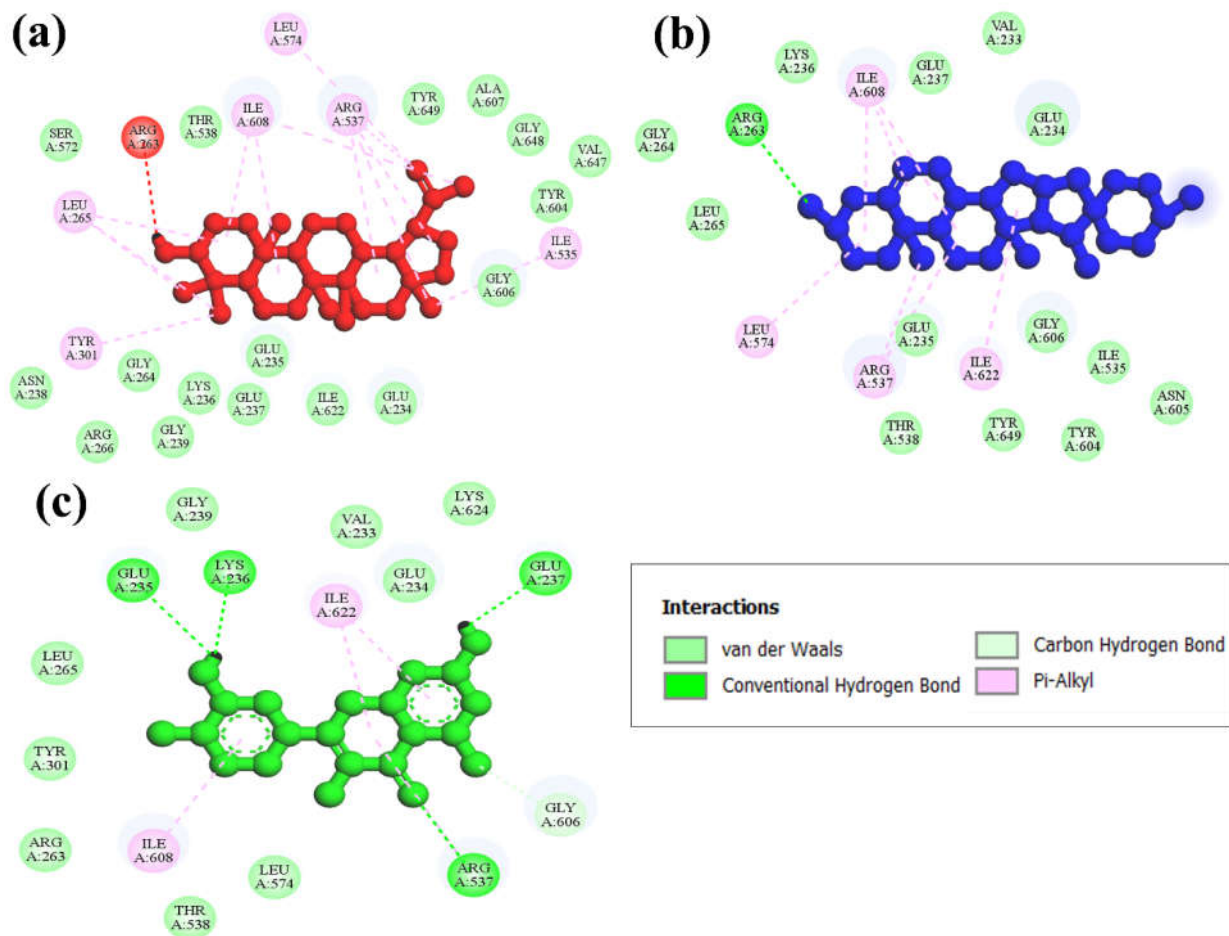
Figure 6. The binding interaction of the ligands with the binding site residues is shown in 2D representation. (**a**) Lupeol, (**b**) Solasodine and (**c**) Quercetin.

3.6. Root Mean Square Deviation

The dynamic stability of the apo-protein over the simulation period of 50 ns was analyzed using the backbone RMSD, as illustrated in Figure 7. The RMSD of the apo-protein exhibits initial fluctuations, and small peaks were observed throughout the simulation period and remained within 1 nm throughout the entire simulation period. The RMSD of the apo-protein and ligand-bound protein complexes was further examined to assess the effect of the ligands on the protein. All the ligand complexes exhibited lower RMSD values than the apo-protein. The Lupeol–protein complex exhibited an initial deviation of 1.5 nm up to 20 ns and stabilized after 30 ns with an RMSD reaching around 1 nm. The Quercetin–protein complex showed less deviation than apo-protein throughout the simulation time. The RMSD of the Quercetin–protein complex remained within 0.75 nm until the end of the simulation period. The Solasodine complex showed lesser deviations when compared with the apo-protein in the majority of the time frame; however, the deviations remained within 0.75 nm throughout the time frame. The RMSD of the protein–ligand complexes revealed that all the complexes remained stable throughout the simulation period, since the RMSD of complexes remained less than 2 nm.
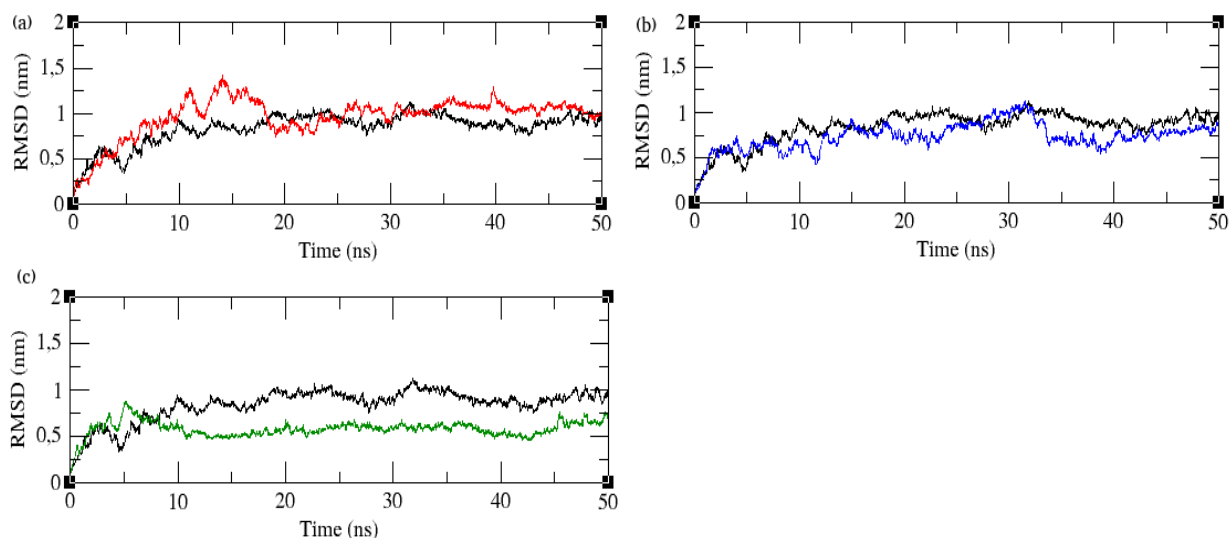
Figure 7. RMSD plot for the backbone carbon atoms of Gingipain R2 protein bound to complexes. (**a**) Lupeol complex. (**b**) Solasodine complex. (**c**) Quercetin complex. Apo-protein is colored black.

3.7. Root Mean Square Fluctuation

The flexibility of the residues in the apo-protein and ligand-bound protein complexes was calculated using RMSF, as shown in Figure 8. The magnitude of the peaks in the RMSF plot describes the flexibility of the residues over the simulation period. The comparison of residual fluctuations revealed that residues from 39 to 568 exhibited smaller fluctuations. The residual fluctuations for residues from 569 to 736 were higher in all ligand-bound protein complexes. Lupeol and Solasodine complexes showed higher residual fluctuations than Quercetin and apo-protein. The lowest residual fluctuation was observed in the Quercetin complex.
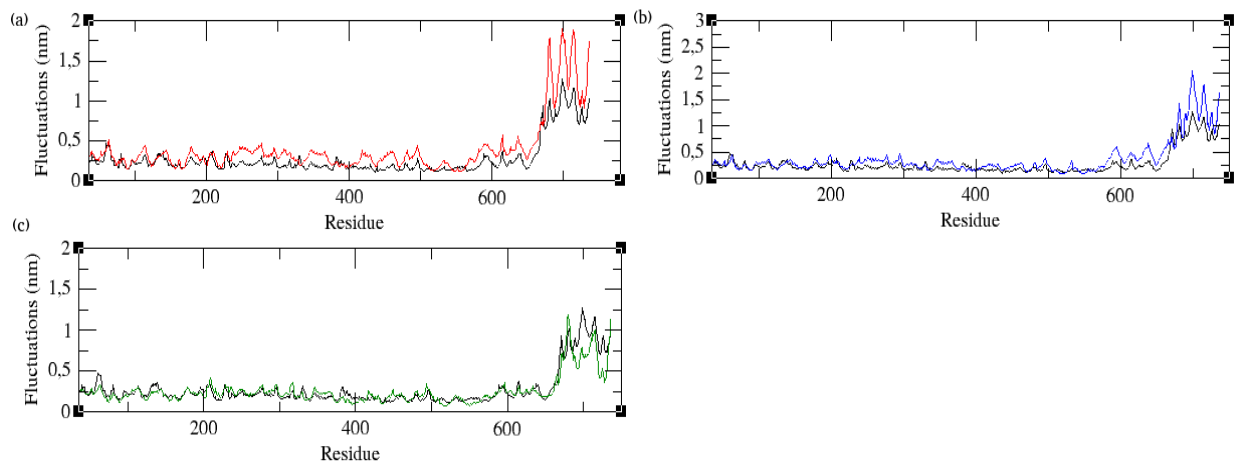

Figure 8. RMSF plot of the residues in Gingipain R2 protein bound to complexes. (**a**) Lupeol complex. (**b**) Solasodine complex. (**c**) Quercetin complex. Apo-protein is colored black.

3.8. Radius of Gyration

The structural stability of all four systems was further assessed using a radius of gyration (Rg). Figure 9 shows the Rg value, which measures the compactness of the protein. The Rg of apo-protein stabilized after 40 ns, indicating its equilibration. The apo-protein Rg converged at 3 nm at the end of the simulation period. The Lupeol complex converged at 3.4 nm at 50 ns. The Lupeol complex showed a higher Rg value than the apo-protein. The binding of Lupeol induced protein flexibility, making the protein less compact. The Solasodine complex exhibited initially high Rg values and converged below the apo-protein

at the end of the simulation. Initially, the binding of Solasodine increased the protein's flexibility; however, as the simulation progressed, the protein became more compact. The Quercetin complex showed a lower Rg at the beginning of the simulation. In the middle of the simulation time period, the Rg value grew above the apo-protein, but at the end, the Rg of Quercetin dropped below the apo-protein. Upon the binding of Quercetin, the compactness of the protein increased initially, but as the simulation proceeded, the protein became flexible. Finally, at the end of the simulation, the complex became compact again. The overall Rg analysis indicated that the binding of Lupeol decreased the compactness of the protein. In contrast, the binding of Quercetin and Solasodine increased the compactness at the end of the simulation time, though they induced initial flexibility.
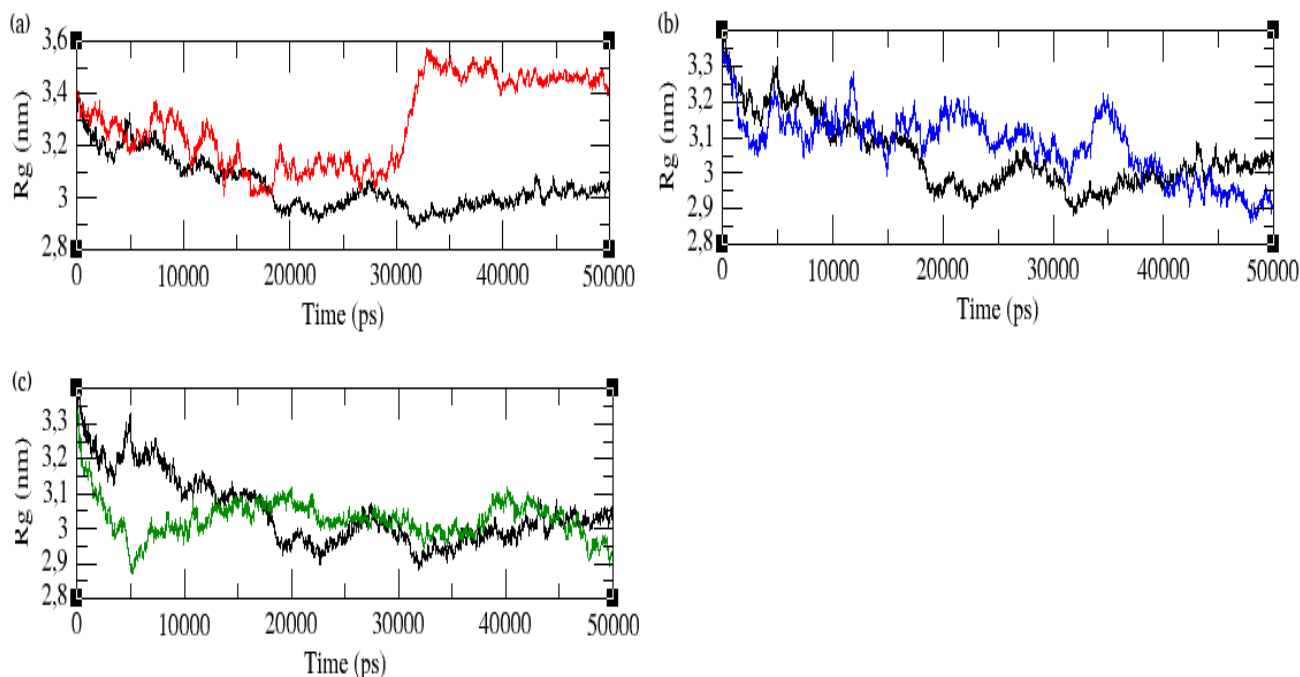

Figure 9. The radius of gyration of Gingipain R2 protein–ligand complexes. (**a**) Lupeol complex. (**b**) Solasodine complex. (**c**) Quercetin complex. Apo-protein is colored black.

3.9. Principal Component Analysis

A principal component analysis was carried out to further assess the compactness and motion of the apo-protein and ligand-bound complexes. The projections of principal components (PC1 and PC2) map the motion of apo-protein and ligand-bound complexes. The mapping of the first two eigenvectors indicated that they account for more than 90% of the motions of the protein backbone atoms, as shown in Figure 10. The comparison of the ligand-anchored complexes with apo-protein indicated that the ligand-to-protein bond has increased the flexibility of the protein by increasing the sampling of phase space coverage.

3.10. Hydrogen Bonds and Interaction Energy Analysis

The hydrogen bonds formed between the protein and ligands indicate their affinity for each other. Lupeol complexes exhibited at least one hydrogen bond throughout the simulation period, although no hydrogen bonds were observed in the starting structure. The Quercetin complex maintained a minimum of one and a maximum of two hydrogen bonds during the 50 ns simulation; however, many hydrogen bonds were lost during the simulation run. The Solasodine complex maintained at least one and a maximum of four hydrogen bonds throughout the simulation time (Figure 11).
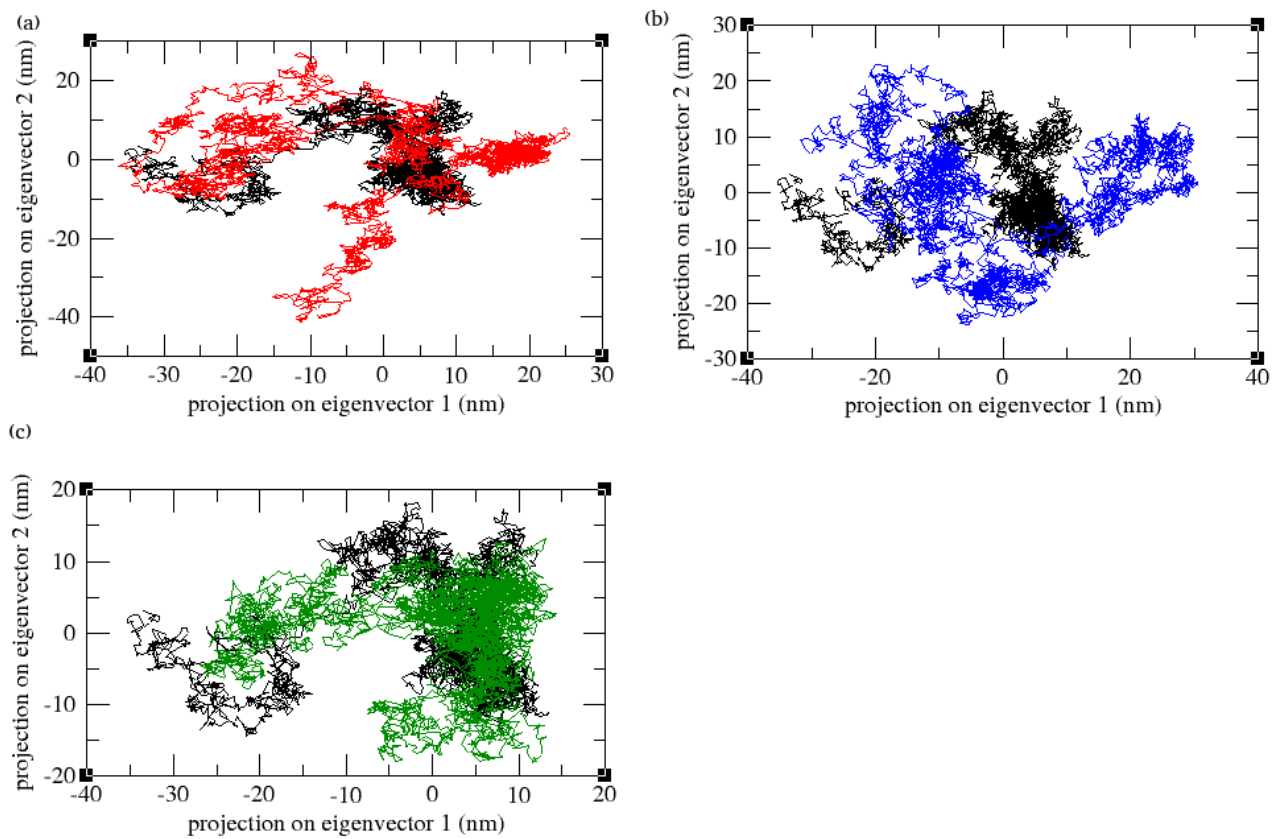
Figure 10. Projection of PC1 and PC2 of Gingipain R2 protein–ligand complexes. (**a**) Lupeol complex (**b**) Solasodine complex. (**c**) Quercetin complex. Apo-protein is colored black.
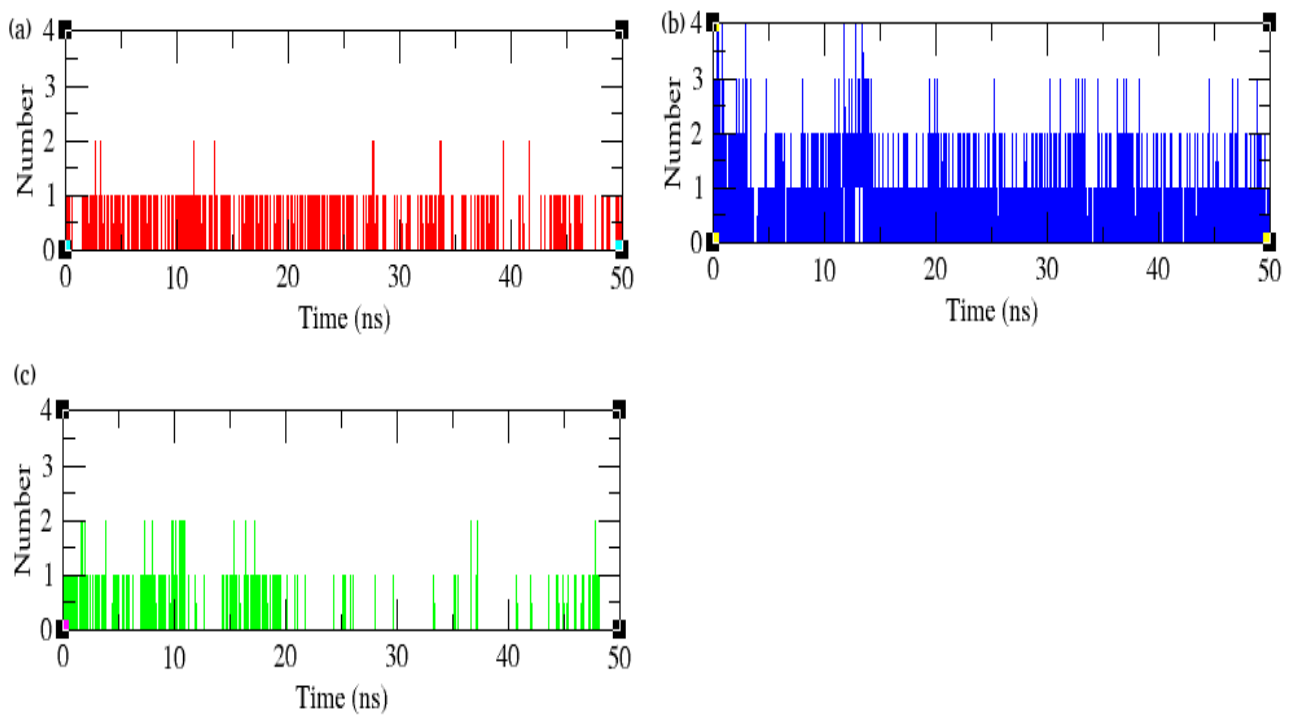

Figure 11. Number of hydrogen bonds formed in the Gingipain R2 protein–ligand complexes. (**a**) Lupeol complex. (**b**) Solasodine complex. (**c**) Quercetin complex.

The three ligand complexes were scored using the MM-PBSA method (Table 6). The comparison of the ligand complexes' binding energies revealed that the Lupeol complex showed higher binding energy than other ligand complexes favoring the formation of non-bonded interactions. All the complexes showed high van der Waals energy compared to other contributors. The comparison of the MDS results of the apo-protein and complexes revealed that the ligand molecules induced structural disturbances upon binding. The overall analysis indicated that the compounds may exhibit the required inhibitory effect on the RgpB protein.

Table 6. MM-PBSA calculations and binding free energy of the protein–ligand complexes.

Complex	Binding Energy kJ/mol	Van der Waals Energy kJ/mol	Electrostatic Energy kJ/mol	Polar Solvation Energy kJ/mol	SASA Energy kJ/mol
Lupeol	-130.003 ± 12.336	-170.912 ± 7.731	-2.223 ± 2.030	61.079 ± 14.458	-17.948 ± 0.931
Quercetin	-103.109 ± 12.604	-169.565 ± 12.181	-6.578 ± 3.867	90.583 ± 19.978	-17.549 ± 0.827
Solasodine	-62.814 ± 18.379	-70.180 ± 9.281	-1.051 ± 5.078	16.112 ± 19.498	-7.694 ± 1.561

4. Side Effects, Limitations and Future Directions

No known severe side effects are reported in the literature for *Solanum xanthocarpum*. In addition, *Sx* is used to manage several ailments in folk medicine [12]. Furthermore, the edible fruits are being cooked and consumed in different parts of India [44,45]. However, studies must be conducted to rule out any possible evidence of cytotoxicity. The limitation of the current study is that a single virulent protein was targeted to prove the interactions of protein and ligands. Further studies with large sample sizes with multiple protein targets in periodontal biofilm need to be evaluated to prove their efficacy. In the future, well-documented clinical trials have to be undertaken to validate their pharmacological actions and eventually for the development of effective chemotherapeutics for the prevention and management of periodontal diseases.

5. Conclusions

The present study demonstrated the pharmacological activities of various *Solanum xanthocarpum* extracts of the fruiting body, including antioxidant, anti-inflammatory and antibacterial activity. Phytochemical components including Solasodine, Lupeol and Quercetin were identified through GC-MS analysis. These components possess potential properties that could be utilized in therapeutics for the prevention and management of periodontal disease. The molecular docking and dynamics analysis also substantiated the phytochemicals' ability to bind and inhibit the function of the RgpB protein of P. gingivalis. Based on our analyses, the current work emphasizes and sheds light on the usage of *S. xanthocarpum* extracts in preventing and treating periodontal diseases. Further investigations to determine its toxicity profile and clinical studies are crucial for broad-spectrum drug discovery.

Author Contributions: Conceptualization, D.A. and G.S.; methodology, D.A. and G.S.; software, D.A., G.S. and B.V.; validation, D.A., G.S. and B.V.; formal analysis, D.A.; investigation, D.A., K.V.A., S.K.B. and P.K.Y.; resources, G.S. and M.I.H.; data curation, D.A. and S.B.; writing—original draft preparation, D.A., G.S., B.V. and R.V.; writing—review and editing, D.A., G.S., S.B. and R.V.; visualization, D.A.; supervision, G.S.; project administration, G.S.; funding acquisition, M.I.H. All authors have read and agreed to the published version of the manuscript.

Institutional Review Board Statement: The study was approved by the Institutional Ethics Committee of Sri Ramachandra Institute of Higher Education and Research (Deemed to be University), Chennai, Tamil Nadu, India (IEC/21/JUN/163/45), and Ragas Dental College and Hospital (no. 20170762).

Informed Consent Statement: Informed consent was obtained from patients.

References

1. Könönen, E.; Gursoy, M.; Gursoy, U.K. Periodontitis: A Multifaceted Disease of Tooth-Supporting Tissues. *J. Clin. Med.* **2019**, *8*, 1135. [CrossRef] [PubMed]
2. Kinane, D.F.; Stathopoulou, P.G.; Papapanou, P.N. Periodontal diseases. *Nat. Rev. Dis. Primers* **2017**, *3*, 17038. [CrossRef] [PubMed]
3. Ferreira, M.C.; Dias-Pereira, A.C.; Branco-de-Almeida, L.S.; Martins, C.C.; Paiva, S.M. Impact of periodontal disease on quality of life: A systematic review. *J. Periodontal. Res.* **2017**, *52*, 651–665. [CrossRef]
4. Lertpimonchai, A.; Rattanasiri, S.; Arj-Ong Vallibhakara, S.; Attia, J.; Thakkinstian, A. The association between oral hygiene and periodontitis: A systematic review and meta-analysis. *Int. Dent. J.* **2017**, *67*, 332–343. [CrossRef]
5. Eivazi, M.; Falahi, N.; Eivazi, N.; Eivazi, M.A.; Raygani, A.V.; Rezaei, F. The Effect of Scaling and Root Planning on Salivary TNF-α and IL-1α Concentrations in Patients with Chronic Periodontitis. *Open Dent. J.* **2017**, *11*, 573–580. [CrossRef]
6. Brookes, Z.L.S.; Bescos, R.; Belfield, L.A.; Ali, K.; Roberts, A. Current uses of chlorhexidine for management of oral disease: A narrative review. *J. Dent.* **2020**, *103*, 103497. [CrossRef]
7. Guerrini, L.; Monaco, A.; Pietropaoli, D.; Ortu, E.; Giannoni, M.; Marci, M.C. Antibiotics in Dentistry: A Narrative Review of Literature and Guidelines Considering Antibiotic Resistance. *Open Dent. J.* **2019**, *13*, 383–398. [CrossRef]
8. Bardají, D.K.R.; Reis, E.B.; Medeiros, T.C.T.; Lucarini, R.; Crotti, A.E.M.; Martins, C.H.G. Antibacterial activity of commercially available plant-derived essential oils against oral pathogenic bacteria. *Nat. Prod. Res.* **2016**, *30*, 1178–1181. [CrossRef]
9. Livada, R.; Shiloah, J.; Tipton, D.A.; Dabbous, M.K. The Potential Role of Curcumin in Periodontal Therapy: A Review of the Literature. *J. Int. Acad. Periodontol.* **2017**, *19*, 70–79.
10. Chandra Shekar, B.R.; Nagarajappa, R.; Suma, S.; Thakur, R. Herbal extracts in oral health care—A review of the current scenario and its future needs. *Pharmacogn. Rev.* **2015**, *9*, 87–92. [CrossRef]
11. Safiaghdam, H.; Oveissi, V.; Bahramsoltani, R.; Farzaei, M.H.; Rahimi, R. Medicinal plants for gingivitis: A review of clinical trials. *Iran. J. Basic Med. Sci.* **2018**, *21*, 978–991. [PubMed]
12. Kumar, S.; Pandey, A.K. Medicinal attributes of Solanum xanthocarpum fruit consumed by several tribal communities as food: An in vitro antioxidant, anticancer and anti HIV perspective. *BMC Complement. Altern. Med.* **2014**, *14*, 112. [CrossRef] [PubMed]
13. Mahalakshmi, P.; Rameshkumar, A.; Sudha, G.; Dineshkumar, T.; Vinoth, H.; Malar, A. Evaluation of anti-microbial properties of Solanum xanthocarpum and Pistacia lentiscus extracts on Streptococcus mutans, Lactobacillus species and Actinomyces viscosus: An in vitro study. *J. Oral MaxillofacPathol.* **2019**, *23*, 383–388.
14. Singh, O.M.; Singh, T.P. Phytochemistry of *Solanum xanthocarpum*: An Amazing Traditional Healer. *J. Sci. Ind. Res.* **2010**, *69*, 732–740.
15. Hajishengallis, G.; Darveau, R.P.; Curtis, M.A. The keystone-pathogen hypothesis. *Nat. Rev. Microbiol.* **2012**, *10*, 717–725. [CrossRef]
16. Lee, S.E.; Hwang, H.J.; Ha, J.S.; Jeong, H.S.; Kim, J.H. Screening of medicinal plant extracts for antioxidant activity. *Life Sci.* **2003**, *73*, 167–179. [CrossRef]
17. Shinde, U.A.; Phadke, A.S.; Nair, A.M.; Mungantiwar, A.A.; Dikshit, V.J.; Saraf, M.N. Membrane stabilizing activity—A possible mechanism of action for the anti-inflammatory activity of *Cedrus deodara* wood oil. *Fitoterapia* **1999**, *70*, 251–257. [CrossRef]
18. Papapanou, P.N.; Sanz, M.; Buduneli, N.; Dietrich, T.; Feres, M.; Fine, D.H.; Tonetti, M.S. Periodontitis: Consensus report of workgroup 2 of the 2017 World Workshop on the Classification of Periodontal and Peri-Implant Diseases and Conditions. *J. Clin. Periodontol.* **2018**, *45* (Suppl. 20), S162–S170. [CrossRef]
19. How, K.Y.; Song, K.P.; Chan, K.G. *Porphyromonasgingivalis*: An Overview of Periodontopathic Pathogen below the Gum Line. *Front. Microbiol.* **2016**, *7*, 53. [CrossRef]
20. Bostanci, N.; Belibasakis, G.N. *Porphyromonasgingivalis*: An invasive and evasive opportunistic oral pathogen. *FEMS Microbiol. Lett.* **2012**, *333*, 1–9. [CrossRef]
21. Kantyka, T.; Latendorf, T.; Wiedow, O.; Bartels, J.; Gläser, R.; Dubin, G.; Schröder, J.M.; Potempa, J.; Meyer-Hoffert, U. Elafin is specifically inactivated by RgpB from *Porphyromonas gingivalis* by distinct proteolytic cleavage. *Biol. Chem.* **2009**, *390*, 1313–1320. [PubMed]
22. Skottrup, P.D.; Leonard, P.; Kaczmarek, J.Z.; Veillard, F.; Enghild, J.J.; O'Kennedy, R.; Sroka, A.; Clausen, R.P.; Potempa, J.; Riise, E. Diagnostic evaluation of a nanobody with picomolar affinity toward the protease RgpB from *Porphyromonasgingivalis*. *Anal. Biochem.* **2011**, *415*, 158–167. [CrossRef] [PubMed]
23. UniProt: A hub for protein information. *Nucleic Acids Res.* **2015**, *43*, D204–D212. [CrossRef]
24. Jumper, J.; Evans, R.; Pritzel, A.; Green, T.; Figurnov, M.; Ronneberger, O.; Hassabis, D. Highly accurate protein structure prediction with AlphaFold. *Nature* **2021**, *596*, 583–589. [CrossRef]
25. Laskowski, R.A.; MacArthur, M.W.; Moss, D.S.; Thornton, J.M. PROCHECK: A program to check the stereochemical quality of protein structures. *J. Appl. Cryst.* **1993**, *26*, 283–291. [CrossRef]

26. Kim, S.; Chen, J.; Cheng, T.; Gindulyte, A.; He, J.; He, S.; Bolton, E.E. PubChem in 2021: New data content and improved web interfaces. *Nucleic Acids Res.* **2021**, *49*, D1388–D1395. [CrossRef]

27. Van Der Spoel, D.; Lindahl, E.; Hess, B.; Groenhof, G.; Mark, A.E.; Berendsen, H.J.C. GROMACS: Fast, flexible, and free. *J. Comput. Chem.* **2005**, *26*, 1701–1718. [CrossRef]

28. Van Aalten, D.M.; Bywater, R.; Findlay, J.B.; Hendlich, M.; Hooft, R.W.; Vriend, G. PRODRG, a program for generating molecular topologies and unique molecular descriptors from coordinates of small molecules. *J. Comput. Aided Mol. Des.* **1996**, *10*, 255–262.

29. Kumari, R.; Kumar, R. Open Source Drug Discovery Consortium, Lynn A. g_mmpbsa—A GROMACS tool for high-throughput MM-PBSA calculations. *J. Chem. Inf. Model.* **2014**, *54*, 1951–1962. [PubMed]

30. Muruhan, S.; Selvaraj, S.; Viswanathan, P.K. In vitro antioxidant activities of *Solanum surattense* leaf extract. *Asian Pac. J. Trop. Biomed.* **2013**, *3*, 28–34. [CrossRef]

31. Narayanan, M.; Jayashree, T.; Kandasamy, S.; Natarajan, D.; Liu, G.; Elesawy, B.H.; Pugazhendhi, A. An in vitro investigation of the antidermatophytic, antioxidant, and nephroprotective activity of *Solanum surattense*. *Process Biochem.* **2021**, *109*, 178–185. [CrossRef]

32. Prasad, K.N.; Yang, B.; Dong, X.; Jiang, G.; Zhang, H.; Xie, H.; Jiang, Y. Flavonoid contents and antioxidant activities from *Cinnamomum* species. *Innov. Food Sci. Emerg. Technol.* **2009**, *10*, 627–632. [CrossRef]

33. Gabay, O.; Sanchez, C.; Salvat, C.; Chevy, F.; Breton, M.; Nourissat, G.; Berenbaum, F. Stigmasterol: A phytosterol with potential anti-osteoarthritic properties. *Osteoarthr. Cartil.* **2010**, *18*, 106–116. [CrossRef]

34. Saleem, M. Lupeol, A Novel Anti-inflammatory and Anti-cancer Dietary Triterpene. *Cancer Lett.* **2009**, *285*, 109–115. [CrossRef]

35. Sathasivam, A.; Muthuselvam, M.; Rajasekaran, R. P10 (IN)—Analysis of phyto chemical constituents and anti-microbial activety of some southern Indian medicinal plants. *J. Pharm. Res.* **2010**, *3*, 1841–1843.

36. Abbas, K.; Niaz, U.; Hussain, T.; Saeed, M.A.; Javaid, Z.; Idrees, A.; Rasool, S. Anti-microbial activity of fruits of Solanum nigrum and *Solanum xanthocarpum*. *Acta Pol. Pharm.* **2014**, *71*, 415–421.

37. Ahmad Khan, M.; Sarwar, A.H.M.G.; Rahat, R.; Ahmed, R.S.; Umar, S. Stigmasterol protects rats from collagen induced arthritis by inhibiting proinflammatory cytokines. *Int. Immunopharmacol.* **2020**, *85*, 106642. [CrossRef] [PubMed]

38. Araldi, E.; Fernández-Fuertes, M.; Canfrán-Duque, A.; Tang, W.; Cline, G.W.; Madrigal-Matute, J.; Suárez, Y. Lanosterol modulates TLR4 mediated innate immune responses in macrophages. *Cell Rep.* **2017**, *19*, 2743–2755. [CrossRef]

39. Jiao, F.; Tan, Z.; Yu, Z.; Zhou, B.; Meng, L.; Shi, X. The phytochemical and pharmacological profile of taraxasterol. *Front. Pharmacol.* **2022**, *13*, 927365. [CrossRef]

40. Santos, C.C.D.M.P.; Salvadori, M.S.; Mota, V.G.; Costa, L.M.; de Almeida, A.A.C.; de Oliveira, G.A.L.; de Almeida, R.N. Antinociceptive and Antioxidant Activities of Phytol In Vivo and In Vitro Models. *Neurosci. J.* **2013**, *2013*, 949452. [CrossRef]

41. Mooney, E.C.; Holden, S.E.; Xia, X.J.; Li, Y.; Jiang, M.; Banson, C.N.; Sahingur, S.E. Quercetin Preserves Oral Cavity Health by Mitigating Inflammation and Microbial Dysbiosis. *Front. Immunol.* **2021**, *12*, 774273. [CrossRef] [PubMed]

42. Corega, C.; Vaida, L.; Festila, D.G.; Rigoni, G.; Albanese, M.; D'Agostino, A.; Bertossi, D. The benefits of Quercitin for dentistry and maxillofacial surgery: A systematic review. *Minerva Stomatol.* 2014; ahead of print.

43. Patel, K.; Singh, R.B.; Patel, D.K. Medicinal significance, pharmacological activities, and analytical aspects of solasodine: A concise report of current scientific literature. *J. Acute Dis.* **2013**, *2*, 92–98. [CrossRef]

44. Revathi, P.; Parimelazhagan, T. Traditional knowledge on medicinal plants used by the Irula tribe of *Hasanur hills*, Erode District, Tamil Nadu, India. *Ethnobot Leaflets.* **2010**, *14*, 136–160.

45. Narayanan, M.K.R.; Anilkumar, N.; Balakrishnan, V.; Sivadasan, M.; Alfarhan, H.A.; Alatar, A.A. Wild edible plants used by the *Kattunaikka*, *Paniya* and *Kuruma tribes* of Wayanad District, Kerala, India. *J. Med. Plants Res.* **2011**, *5*, 3520–3529.